

METHOD

Identification and classification of common RNA structure motifs

Martin A Smith^{1,2*}†, Stefan E Seemann^{3†}, XiuCheng Queck^{1,2} and John S Mattick^{1,2}

*Correspondence:
m.smith@jaggar.org.au

¹RNA Biology and Plasticity Group,
Garvan Institute of Medical Research,
384 Victoria Street, NSW 2010
Sydney, Australia

Full list of author information is
available at the end of the article

†Contributed equally

Abstract

The diversity of processed transcripts in eukaryotic genomes poses a challenge for the classification of their biological functions. Sparse sequence conservation in non-coding sequences and the unreliable nature of RNA structure predictions further exacerbate this conundrum. Here, we describe a computational method for the unsupervised discovery and classification of homologous RNA structure motifs from a set of sequences of interest. Our approach outperforms other tools at classifying known RNA structure families, both in time and accuracy. It identifies clusters of known and novel structure motifs from ENCODE immuno-precipitation data of 44 RNA-binding proteins.

Keywords: Functions of RNA structures; RNA structure clustering; Machine learning; RNA–protein interactions; Functional genome annotation; Regulation by non-coding RNAs

Background

As genomic technologies progress, an ever increasing amount of non-protein coding RNAs (ncRNA) are being discovered. Long noncoding RNAs (lncRNAs) are of particular interest for functional genome annotation given their abundance throughout the genome. So far, few lncRNAs have been functionally characterised, and those that have seem to be involved in regulation of gene expression and epigenetic states [1, 2]. Understanding the molecular mechanisms underlying the biological functions of lncRNAs – and how they are disrupted in disease – is required to improve the functional annotation of the human genome.

Many ncRNAs lack sequence conservation or sequence motifs, in contrast to protein-coding genes. Most small ncRNAs have well characterised secondary and tertiary structures, as evidenced in RFAM, the largest collection of curated RNA families (2,588 families as of version 12.2 [3]). In contrast, determining the structural features of lncRNAs is a complex problem given their size and, in general, faster evolutionary turnover. These challenges have raised doubts concerning the prevalence of functional structural motifs in lncRNAs [4, 5], despite evolutionary and biochemical support of conserved base pairing interactions [6, 7, 8]. Nonetheless, the higher-order structure of RNA molecules is an essential feature of ncRNAs that can be used for their classification and the inference of their biological function. We, and others, hypothesise that lncRNAs act as scaffolds for the recruitment of proteins and assembly of ribonucleoproteins (RNPs), mediated by the presence of modular RNA structures, akin to the domain organisation of proteins [9, 10, 11, 12, 6, 13, 14]. Protein-interacting regions of lncRNAs are likely to contain a combination of sequence and structure motifs that confer binding specificity, which may be present in multiple target transcripts. For example, there is evidence that sequence and structure components

of transposable elements, which are frequent in lncRNAs [?, ?], have been co-opted into mammalian gene regulatory networks [?, ?].

Identifying RNAs with similar functions involves comparing both their primary sequence and higher-order structures simultaneously. However, sequence-based methods to identify common structural features perform poorly when sequence identity falls below 60% [15]. Hence, methods are needed that find structural similarity independent from sequence conservation and freed from single RNA secondary structure predictions. The Sankoff algorithm resolves the optimal sequence-structure alignment of two RNAs [16], but its computational complexity limits its practicality. Alternative strategies often employ pre-calculated secondary structure ensembles for each sequence, e.g. base pair probabilities in thermodynamically equilibrated RNA structure ensembles [17]. The latter can substantially speed up the calculation of structure-based alignments [18], of which there are many variants. The programs PMcomp [18], LocaRNA [19], and ProbAlign [20] use the pre-computed base pair probability matrices of both sequences and score the alignment based on the notion of a common secondary structure. The sequence-structure alignment problem is reduced to a two-dimensional problem by RNAPALN [21] and StrAL [22], which reduce base pair probabilities to base specific probabilities (such as a base-wise unpaired probability). All these methods fail to explicitly consider suboptimal structures in the alignment. The pairwise alignment of base pairing probability matrices (RNA dot plots) was first introduced by CARNA [23, 24], which iteratively improves alignments using a constraint programming technique implementing a branch and bound scheme. Another heuristic is pruning of the dynamical programming matrix without pre-folding constraints, as implemented by FoldAlign [25, 26].

Will *et al.* first showed that a (dis)similarity matrix can be constructed from all-vs-all pairwise RNA structure alignments with the pairwise alignment tool LocaRNA, identifying known and novel groups of homologous RNAs using hierarchical clustering [19]. However, this strategy involves applying a subjective threshold to the resulting dendrogram to extract structurally related sequences. Alternative methods to identify clusters of homologous RNAs include NoFold, which clusters query sequences based on their relative similarity to a panel of reference structure motif profiles [27], and GraphClust, an alignment-free approach that decomposes RNA structures into graph-encoded features [28]. RNAscClust, an extension of GraphClust, utilises the evolutionary signatures of RNA structures as additional classification feature [29].

Here, we describe a computational pipeline for the identification and classification of homologous RNA structures from a large set of query sequences. At its core lies DotAligner, a heuristic pairwise sequence alignment algorithm that considers an ensemble of suboptimal base pairing probabilities for each queried sequence. We compare DotAligner with other pairwise RNA structure alignment algorithms to highlight its speed and accuracy at classifying known RNA families. We combine DotAligner with density based clustering for the impartial identification of RNA structural motifs, which can identify known RFAM families and novel RNA structural motifs from ENCODE eCLIP data. The resulting clusters of homologous RNA structures can then be used to search for homologous structures across reference genomes and transcriptomes to generate a map of functionally related RNA structure motifs.

Results

Ensemble-guided pairwise RNA structure alignment

DotAligner leverages the diversity of suboptimal solutions from a partition function of RNA secondary structure predictions to identify an optimal sequence-structure alignment of two RNAs. The algorithm overcomes the limitations of comparing unique RNA secondary structures (such as minimum free energy predictions) to yield a (near) optimal sequence alignment that considers mutual base pair probabilities. Figure 1 illustrates a structural alignment performed with DotAligner in contrast to an alignment that considers only sequence composition. A major criteria for the implementation was a fast running time to make DotAligner applicable for RNA structure clustering of large data sets. Consistently, the algorithm performs pairwise sequence-structure alignments from pre-calculated RNA dot plots using an alignment-envelope heuristic, which impose constraints on sub-optimal string alignments, and fold-envelope heuristics, which impose constraints to pre-calculated base pairing probabilities. The alignment procedure thus consists of two steps, each considering base pairing probabilities: (i) Computation of a partition function over all canonical pairwise string alignments, and (ii) structure-weighted stochastic backtracking of all sequence alignments. The detailed implementation and mathematical description of DotAligner can be found in the Supplementary Methods.

We first tested DotAligner on BRAliBase 2.1 pairwise RNA structure alignments, a reference dataset specifically designed for algorithm benchmarking [15, 30] (see Methods). In this application, DotAligner seemingly performs worse than three other state of the art algorithms, namely CARNA [24], FOLDALIGN [31, 32] and LocaRNA [19] (Fig. 2). Interestingly, many of the pairwise structure alignments produced Structural Conservation Index (SCI) scores above those from the BRAliBase 2.1 reference alignments (Fig. 2B). The SCI represents the alignment consensus energy normalized by the average energy of the single sequences folded independently [33]; it has been shown to be one of the most reliable metrics for conserved RNA structure detection [34]. With the exception of DotAligner, all other surveyed algorithm produce a substantial amount of alignments with SCI values above that of the reference alignment (Fig. 2B), suggesting that many optimization algorithms tend to overestimate the amount of paired bases in consensus RNA structure predictions.

Fast and accurate classification of RNA structures

The intended application of DotAligner is the identification and classification of RNA structural motifs from a large and diverse set of sequences of interest. Therefore, we evaluated the ability of DotAligner to distinguish between distinct structured RNA species from a heterogeneous sample of known RNA structure families. We performed all versus all pairwise structure alignments of stochastically sampled RFAM sequences, which were selected with constraints on their sequence composition (PID) to control for and ascertain any sequence-dependent biases (see Methods). DotAligner alignment scores were then compared to a binary classification matrix representing the distinct RFAM families (Supplementary Figure 1).

Despite the seemingly poor quality of pairwise alignments generated by DotAligner, it reproduces the known classification of RFAM structures more accurately than all other surveyed pairwise RNA structure alignment tools (Fig. 3A-C). Only CARNA, another ensemble-based structural alignment algorithm, presents classification accuracies comparable to DotAligner. However, CARNA requires substantially more time to perform the comparisons (Fig. 3D) as it will indefinitely continue to compute the alignment until it converges on an optimal result, or a hard time constraint is enforced. In this regard, DotAligner performs better than all other RNA structure alignment tools, highlighting the efficacy of the implemented heuristics it employs. In contrast, the heuristics implemented in RNAlign increased the speed of pmcomp by 2 orders of magnitude, but at a slight reduction in accuracy (Fig. 3C,D). Only a C++ implementation of the Needleman-Wunsch Algorithm (NWA) [35]—a classical sequence alignment algorithm that ignores secondary structure information—performs faster than DotAligner on average, most likely due to the presence of stretches of homologous sequences within biologically related RNAs.

Density-based clustering of homologous RNA structures

Given DotAligner's accurate classification of known structured RNA, we subjected its output to cluster analysis to identify and extract input sequences which display common sequence-structure motifs. The previous work by Will *et al.* applied hierarchical clustering to the dissimilarity matrices produced by LocaRNA to organise sequences based on their structural homology [19]. However, this does not apply a cut-off that can be used to extract meaningful clusters of structurally homologous sequences in an unsupervised manner. We attempted to achieve this by applying a statistical threshold derived from bootstrapping the underlying data using pvclust [36], but this generated clusters of variable size that often spanned across many disjoint families (data not shown).

We therefore opted for a density-based clustering strategy that, in theory, can decipher clusters of varying density (i.e. subsets of the data with greater sequence-structure homology). The OPTICS (Ordering Points To Identify the Clustering Structure) algorithm [37] was chosen for this purpose, as it has very few parameters to optimise. OPTICS is a derivative of the Density-Based Clustering for Application with Noise (DBSCAN) [38] algorithm that, as its name states, is suitable for noisy data, such as RNA immunoprecipitation followed by high-throughput sequencing (RIPSeq). We benchmarked the two main OPTICS clustering parameters—Xi steepness threshold and the minimum number of points in a cluster (Supplementary Fig. 2)—on a pooled set of 580 stochastically sampled RFAM sequences encompassing various ranges of sequence similarity, as well as a corresponding set of 580 dinucleotide shuffled controls (see Methods). After performing all vs all pairwise alignments with DotAligner, we evaluated the effect of OPTICS parameters on clustering performance, revealing that a minimum of 4 points (or sequences) and a steepness threshold of 0.006 gave the best results (Supplementary Fig. 1A).

GraphClust, the combination of DotAligner and OPTICS performs comparably well (Fig. 4, Table 1, Supplementary Table 1). The default version of NoFold nonetheless outshines DotAligner at clustering known RFAM families. However, it intrinsically employs RFAM covariance models (CMs) that are also present in the test data, therefore this specific application is likely to be subject to over-fitting. We thus removed the CMs associated

to the RFAM sequences in our benchmarking dataset from the NoFold algorithm, which yielded lower sensitivity and less accurate qualitative cluster metrics than the DotAligner and OPTICS combination, while its specificity increased slightly despite removing 72 CMs from its classification set.

Identifying protein-binding RNA motifs from eCLIP data

The optimised parameters for OPTICS clustering of DotAligner output were incorporated into a high-performance computing pipeline that extracts clusters of homologous RNA structural motifs from a set of input sequences (see Methods). This pipeline was applied to enhanced cross-linked RNA immunoprecipitation (eCLIP) sequencing data from 44 RNA binding proteins from the ENCODE consortium [39], with 100 positive control sequences from RFAM (Supplementary Table 2). From 2,750 high-confidence ($>8x$ fold-enrichment vs background, P-value $< 10^{-4}$) eCLIP peaks that overlap evolutionarily conserved secondary structure predictions, 25 significant clusters of homologous RNA were detected, including all 11 positive controls (Fig. 5).

Indeed, the *spike in* RFAM sequences facilitate the identification of similar RNA structures, such as the homologs to snoRNA72 depicted in (Fig. 5C-D). The 4 additional sequences that co-cluster with the RFAM 72 controls are all associated to the DKC1 protein, which binds to H/ACA snoRNAs. Furthermore, 3 of the DKC1-bound beaks are annotated as snoRNAs in the Gencode 24 reference, while the 4th is not annotated as a snoRNA despite strong sequence and structure similarity, highlighting how this method can successfully identify and classify new RNA structure motifs. Another example is the Y RNA cluster, which contains 3 sequences homologous to this RFAM family that are also associated to the TROVE2 protein, which binds to misfolded non-coding RNAs, pre-5S rRNA, and Y RNAs.

Our method also identifies RNA structure families impartially, as exemplified by several clusters of DKC1-associated sequences which present consensus secondary structures indicative of snoRNAs (Fig. 5E). Closer inspection of the corresponding eCLIP peaks revealed that these sequences are indeed annotated as snoRNAs in Gencode. There are also examples of de novo structural motifs that are associated to RNA-binding proteins with no previously known binding sites, such as an UPF1-dominated cluster (Fig. 5F), composed of a structure motif belonging to ALU repeats (Supplementary Fig. 3). When searching the human genome for homology to the RNA structure motif derived from this cluster, most ALU elements are detected, as well as a few other repeat-containing sequences. Interestingly, 998 homologs to the motif did not localise to ALU elements (Supplementary Figure 3B), 58% of which overlap miTranscriptome reference transcripts [40].

Discussion

As the increasing accessibility of next generation sequencing coalesces with precision medicine, in-depth transcriptome profiling will help elucidate the function and clinical impact of disease-associated, non-coding single nucleotide variants. Indeed, 80% of disease-associated single nucleotide polymorphisms occur in non-coding regions [41, 42]. Thus, elucidating the structural features of RNAs associated to RNA-binding proteins and ribonucleoprotein (RNP) complexes, combined to the systematic classification of their genome-wide occurrence, can identify novel riboSNitches (functional RNA structures that are disrupted in disease) and help pinpoint the molecular function of non-coding mutations. The

structural diversity of some RNAs, especially of riboswitches, allows them to respond to their environment (such as temperature change) which may provide alternative binding sites for proteins. By considering the suboptimal structure potential of RNAs, DotAligner is suitable for exploring RNA molecules of similar suboptimal features.

Given its relative speed and accuracy, DotAligner can be used to generate larger (dis)similarity matrices for cluster analysis than other pairwise structure alignment algorithms, or at least produce them with reasonable computational power. In addition to its speed, the strength of DotAligner lies in its capacity to accurately score structurally homologous RNA sequences. The algorithm appears to generate pairwise alignments that differ qualitatively to the reference structural alignments. Despite this, DotAligner can harness the information content of base pair probability ensembles to output a reliable structural similarity score of two RNA sequences, reducing several dimensions of information content into a single discriminative numeric value. Our results show that this can nonetheless be sufficient to extract structurally and functionally related sequences from a large amount of noisy input; an ideal application for screening high-throughput sequencing data—such as RNA immunoprecipitation data—for common structural motifs.

High-throughput CLIPseq data poses a challenge for consensus motifs detection since several molecules that are in close physical proximity to the target molecule get co-precipitated together. Consequently, other RNA sequences may be present that do not directly bind to the target protein. We have shown that our method is nonetheless suitable for such noisy biological data. For example, the UPF1 cluster we describe may be an example of an indirect binding event, as UPF1 directly interacts with STAUF1, a double stranded RNA-binding protein which has been reported to target ALU sequences [43]. There are also additional clusters identified in our eCLIP analysis where sequences from more than one target protein cluster together, which raises the possibility that a common RNA structure motif may be bound by two different proteins, either as part of a quaternary complex or as a common, competing binding target. We privilege this hypothesis over one of spurious false-positive clustering given our benchmark results and the observation that very few clusters were observed when analysing less stringently filtered eCLIP peaks (not shown).

DotAligner has several parameters that will influence the clustering results and speed depending on the type of input data. The most influential variables are the weight between sequence and structure similarity, and the exploration depth of the suboptimal alignments in the stochastic backtracking. Here, we present the best trade-off between alignment accuracy and speed based on a collection of RFAM seed alignments, and show that these default settings are applicable on de-novo data from an eCLIP experiment.

A greater challenge lies in the accurate depiction of RNA structure motif boundaries. Whereas global structures may stabilize the RNA molecule, local structural domains are often sufficient for recognition by RNA binding proteins. When compared to LocaRNA, DotAligner calculates semi-local alignments by introducing penalty-free gaps at the sequence extremities. However, this approach optimises only the pairwise local similarity score, but it does not explore suboptimal alignments for optimal cluster construction. This could be done in the DotAligner framework but would dramatically increase search space

and run-time. We circumvented this issue by overlapping eCLIP peaks to evolutionarily conserved RNA secondary structure predictions with well-characterised flanking helices supported by base pair covariation [6]. While preparing this manuscript, a complementary and comprehensive dataset of evolutionarily conserved RNA secondary structures was published [44], which could also increase the amount of eCLIP peaks with accurate structural motif boundaries. Alternatively, RNA structure boundaries can be refined using alternative strategies such as computational boundary refinement with LocaRNA-P [45], or improving the biological data with enzymatic probing with the double-stranded RNase T1 endoribonuclease, for example.

Conclusion

An efficient pairwise RNA sequence alignment heuristic, which intrinsically considers sub-optimal base pairings, accurately discriminates between distinct structured RNAs families. When combined to a noise tolerant density based clustering algorithm, this approach identifies known and novel RNA structure motifs from a set of input sequences without a priori knowledge. The resulting RNA structure motifs can subsequently be used to identify homologs in reference genomes to improve the annotation of long non-coding RNAs and increase the repertoire of functional genetic elements.

Methods

Benchmarking and parameter optimisation

The DotAligner algorithm implements several theoretical parameters that first need to be tuned before being applied to biological sequence analysis. All combinations of core parameters were tested on the 8,976 pairwise RNA structure alignments curated in the BRAliBase 2.1 reference dataset [30]. For each set of parameter combinations, the amount of alignments producing identical structural topologies to the reference alignment was determined using *RNAdistance*. The Structural Conservation Index (SCI), a robust measure of RNA structural alignment integrity [34] based on Minimum Free Energy (MFE), and the Matthews Correlation Coefficient (MCC) of *predicted* and *reference* RNA secondary structure were also calculated for all resulting alignments:

$$\text{MCC} = \frac{(TP \cdot TN) - (FP \cdot FN)}{\sqrt{(TP + FP)(TP + FN)(TN + FP)(TN + FN)}}$$

$$\Delta\text{SCI} = \text{SCI}_{\text{predicted}} / \text{SCI}_{\text{reference}}, \text{ where } \text{SCI} = \text{MFE}_{\text{consensus}} / \overline{\text{MFE}}_{\text{single}}$$

Baseline parameters were then selected via a product rank of these 2 metrics and subjected to refinement using a binary classification approach, described in the next section.

Classification of RNA secondary structure families

Further refinement of the optimal parameters was performed using a binary classifier for two sets of 200 stochastically sampled RFAM entries with published structures: (i) a low pairwise sequence identity set, and (ii) a high Pairwise Sequence Identity (PSI) set, where any two sequences from the same family share between 0-55% and 56-95% pairwise sequence identity, respectively. The JAVA implementation of this algorithm, derived from [6], can be found in the Supplementary Methods. A binary classification matrix was then constructed, where sequences x and y present a score of 1 if they belong to the same RFAM

family, versus a score of 0 if they do not. The similarity matrix resulting from all-vs-all pairwise comparisons with DotAligner was tested for accuracy using the Area Under the Curve AUC of the ROC, as calculated R package pROC [46]. A more restricted range of parameter values were then tested on both datasets, where a ranked sum for both datasets of the AUC was performed to determine the default runtime parameters for DotAligner, namely T=10 s=1 k=0.3 t=0.5 o=1 e=0.05 (Supplementary Table 3). CARNA version 1.2.5 was run with parameters “–write-structure –noLP –time-limit=120000” ; LocaRNA version 1.7.13 was run with parameter “–noLP”; FOLDALIGN version 2.1.1 was run with and without parameter “-global”. Default parameters were used for pmcomp, downloaded from <https://www.tbi.univie.ac.at/RNA/PMcomp/> and RNApaln version 2.3.5. The custom implementation of Needleman-Wunsch can be found in the GitHub repository associated to this work as well as the benchmark implementation scripts.

Clustering RNA structures with randomised controls

OPTICS benchmarking was performed by stochastically sampling the collection of RFAM 12.0 seed alignments using the JAVA program GenerateRFAMsubsets.java (see Supplementary Methods) with three ranges of pairwise sequence identity: 1-55%, 56-75%, and 75-95%, a minimum of 5 representative sequences per family, and sizes ranging between 70 and 170 nt. The resulting 580 unique sequences were then shuffled while controlling their dinucleotide content with the easel program included in the Infernal (v1.1.2) software package [47] with option ”-k 2”. The 1160 sequences were submitted to all-vs-all pairwise comparisons with DotAligner and the scores were inverted and a normalised (min=1, max=0) into a dissimilarity matrix, which was then imported into the R statistical programming language, converted into a ‘dist’ object without transformation, and subjected to OPTICS clustering as implemented in the ‘dbscan’ CRAN repository with a range of parameters (see Fig. 4A,B).

Other tested RNA clustering approaches were GraphClust and NoFold. We ran GraphClust version 0.7.6 inside the docker image provided with RNAscClust with default parameters. NoFold version 1.0.1 uses 1,973 RFAM covariance models by default as empirical feature space. In the NoFold (all CMs) variant we ran the program with default parameters, whereas in the NoFold (filtered) variant we reduced the feature space to 1,902 covariance models by removing RFAM families from our benchmark set.

The following clustering performance metrics was used:

- True Positives (TP) = Number of representatives from the dominant RFAM family in a cluster;
- False Positives (FP) = Number of non-dominant RFAM family representatives in cluster, or clusters where there is no dominant RFAM family (i.e. equally represented families), or clusters where dominant sequence is a negative control;
- False Negatives (FN) = RFAM sequences that fail to cluster;
- True Negatives (TN) = Negative control sequences that fail to cluster.
- Sensitivity (recall) = $TP / (TP + FN)$;
- Specificity = $TN / (TN + FP)$;
- False positive rate = $1 - \text{Specificity}$;
- Precision = $TP / (TP + FP)$;
- Accuracy = $(TP + TN) / (TP + TN + FP + FN)$;

Clustering of protein-bound evolutionarily-conserved RNAseq reads

The genomic coordinates of ENCODE eCLIP peaks were downloaded in .bed format from the April 2016 release via the ENCODE portal (<https://www.encodeproject.org/search>). The resulting 5,040,096 peaks were filtered to keep only those with $\geq 8x$ fold enrichment over the total input background and an associated P-value $\leq 10^{-4}$. Furthermore, peaks were merged if they overlapped by more than 50nt to avoid over-representing the same sequence (Additional file 1). The remaining peaks were subsequently filtered by retaining only those that present same-strand overlap with any evolutionarily conserved structure (ECS) predictions from [6]. Finally, the associated genomic sequences were extracted into a .fasta file, which was supplemented with 100 reference RNA structures from 11 RFAM families (see Supplementary Table 1). Merging, overlap, and sequence extraction operations were performed with bedtools version v2.26.0.

The normalised similarity matrix resulting from all vs all pairwise comparisons with DotAligner was then subjected to clustering with the dbscan 1.1-1 R package from Michael Hahsler <https://github.com/mhahsler/dbscan> using the command ‘opticsXi (optics(D, eps=1, minPts=4, search="dist"), xi = 0.006, minimum=T)’. The sequences for each cluster were then extracted and submitted to multiple structure alignment with mLocaRNA version 1.9.1 using parameters ‘--probabilistic --iterations=10 --consistency-transformation --noLP’.

Availability of data and materials

Source code, pipelines and data can be obtained at <https://github.com/noncodo/BigRedButton>.

Competing interests

The authors declare that they have no competing interests.

Funding

MAS and JSM are partially supported by a Cancer Council NSW project grant (RG 14-18). SES was supported by a Carlsberg Foundation grant (2011_01_0884) and the Innovation Fund Denmark (0603-00320B).

Author's contributions

MAS, SES and JSM conceived the study. SES and MAS wrote the manuscript and performed data analysis. MAS performed benchmarking analyses and developed analytic pipelines. SES created and implemented DotAligner source code. XQ assisted in DotAligner parameter optimisation and benchmarking.

Acknowledgements

We would like to thank DR Eva Maria Novoa Pardo for her scientific council, R programming tricks, and critical manuscript reading. Thanks to Prof Oliver Mülhemann for discussions relating to data interpretation. Thanks to Luis Renato Arriola-Martinez for his advice concerning covariance models. Thanks to Michael Hahsler for developing and disseminating a fast DBSCAN R package.

Author details

¹RNA Biology and Plasticity Group, Garvan Institute of Medical Research, 384 Victoria Street, NSW 2010 Sydney, Australia. ²St Vincent's Clinical School, Faculty of Medicine, UNSW Australia, NSW 2010 Sydney, Australia. ³Center for non-coding RNA in Technology and Health (RTH), University of Copenhagen, Groennegaardsvej 3, 1870 Frederiksberg, Denmark.

References

1. Morris, K.V., Mattick, J.S.: The rise of regulatory rna. *Nature Reviews Genetics* **15**(6), 423–437 (2014)
2. Engreitz, J.M., Ollikainen, N., Guttman, M.: Long non-coding rnas: spatial amplifiers that control nuclear structure and gene expression. *Nature Reviews Molecular Cell Biology* (2016)
3. Nawrocki, E.P., Burge, S.W., Bateman, A., Daub, J., Eberhardt, R.Y., Eddy, S.R., Floden, E.W., Gardner, P.P., Jones, T.A., Tate, J., et al.: Rfam 12.0: updates to the rna families database. *Nucleic acids research* **43**(D1), 130–137 (2015)
4. Eddy, S.R.: Computational analysis of conserved rna secondary structure in transcriptomes and genomes. *Annual review of biophysics* **43**, 433–456 (2014)
5. Rivas, E., Clements, J., Eddy, S.R.: A statistical test for conserved rna structure shows lack of evidence for structure in lncrnas. *Nature Methods* (2016)
6. Smith, M.A., Gesell, T., Stadler, P.F., Mattick, J.S.: Widespread purifying selection on rna structure in mammals. *Nucleic acids research*, 596 (2013)
7. Spitale, R.C., Flynn, R.A., Zhang, Q.C., Crisalli, P., Lee, B., Jung, J.-W., Kuchelmeister, H.Y., Batista, P.J., Torre, E.A., Kool, E.T., et al.: Structural imprints in vivo decode rna regulatory mechanisms. *Nature* **519**(7544), 486–490 (2015)

8. Lu, Z., Zhang, Q.C., Lee, B., Flynn, R.A., Smith, M.A., Robinson, J.T., Davidovich, C., Gooding, A.R., Goodrich, K.J., Mattick, J.S., et al.: Rna duplex map in living cells reveals higher-order transcriptome structure. *Cell* **165**(5), 1267–1279 (2016)
9. Zappulla, D., Cech, T.: Rna as a flexible scaffold for proteins: yeast telomerase and beyond. In: Cold Spring Harbor Symposia on Quantitative Biology, vol. 71, pp. 217–224 (2006). Cold Spring Harbor Laboratory Press
10. Hogg, J.R., Collins, K.: Structured non-coding rnas and the rnp renaissance. *Current opinion in chemical biology* **12**(6), 684–689 (2008)
11. Rinn, J.L., Chang, H.Y.: Genome regulation by long noncoding rnas. *Annual review of biochemistry* **81**, 145–166 (2012)
12. Mercer, T.R., Mattick, J.S.: Structure and function of long noncoding rnas in epigenetic regulation. *Nature structural & molecular biology* **20**(3), 300–307 (2013)
13. Chujo, T., Yamazaki, T., Hirose, T.: Architectural rnas (arcrnas): A class of long noncoding rnas that function as the scaffold of nuclear bodies. *Biochimica et Biophysica Acta (BBA)-Gene Regulatory Mechanisms* **1859**(1), 139–146 (2016)
14. Blythe, A.J., Fox, A.H., Bond, C.S.: The ins and outs of lncrna structure: How, why and what comes next? *Biochimica et Biophysica Acta (BBA)-Gene Regulatory Mechanisms* **1859**(1), 46–58 (2016)
15. Gardner, P.P., Wilm, A., Washietl, S.: A benchmark of multiple sequence alignment programs upon structural {RNAs}. *Nucleic Acids Res* **33**(8), 2433–2439 (2005). doi:[10.1093/nar/gki541](https://doi.org/10.1093/nar/gki541)
16. Sankoff, D.: Simultaneous solution of the {RNA} folding, alignment and protosequence problems. *SIAM J. Appl. Math.* **45**, 810–825 (1985)
17. McCaskill, J.S.: The equilibrium partition function and base pair binding probabilities for {RNA} secondary structure. *Biopolymers* **29**(6-7), 1105–1119 (1990). doi:[10.1002/bip.360290621](https://doi.org/10.1002/bip.360290621)
18. Hofacker, I.L., Bernhart, S.H., Stadler, P.F.: Alignment of RNA base pairing probability matrices. *Bioinformatics* **20**(14), 2222–2227 (2004). doi:[10.1093/bioinformatics/bth229](https://doi.org/10.1093/bioinformatics/bth229)
19. Will, S., Reiche, K., Hofacker, I.L., Stadler, P.F., Backofen, R.: Inferring noncoding RNA families and classes by means of genome-scale structure-based clustering. *PLoS Comput Biol* **3**(4), 65 (2007). doi:[10.1371/journal.pcbi.0030065](https://doi.org/10.1371/journal.pcbi.0030065)
20. Roshan, U., Livesay, D.R.: Probaalign: multiple sequence alignment using partition function posterior probabilities. *Bioinformatics* **22**(22), 2715–2721 (2006). doi:[10.1093/bioinformatics/btl472](https://doi.org/10.1093/bioinformatics/btl472)
21. Lorenz, R., Bernhart, S.H., Höner Zu Siederdissen, C., Tafer, H., Flamm, C., Stadler, P.F., Hofacker, I.L.: ViennaRNA package 2.0. *Algorithms Mol Biol* **6**, 26 (2011). doi:[10.1186/1748-7188-6-26](https://doi.org/10.1186/1748-7188-6-26)
22. Dalli, D., Wilm, A., Mainz, I., Steger, G.: STRAL: progressive alignment of non-coding RNA using base pairing probability vectors in quadratic time. *Bioinformatics* **22**(13), 1593–1599 (2006). doi:[10.1093/bioinformatics/btl142](https://doi.org/10.1093/bioinformatics/btl142)
23. Palù, A., Möhl, M., Will, S.: A Propagator for Maximum Weight String Alignment with Arbitrary Pairwise Dependencies. In: Cohen, D. (ed.) *Principles and Practice of Constraint Programming – CP 2010*, Lecture no edn., pp. 167–175 (2010). doi:[10.1007/978-3-642-15396-9_16](https://doi.org/10.1007/978-3-642-15396-9_16). http://dx.doi.org/10.1007/978-3-642-15396-9_16
24. Sorescu, D.A., Möhl, M., Mann, M., Backofen, R., Will, S.: CARNA—alignment of RNA structure ensembles. *Nucleic acids research* **40**(Web Server issue), 49–53 (2012). doi:[10.1093/nar/gks491](https://doi.org/10.1093/nar/gks491)
25. Havgaard, J.H., Torarinsson, E., Gorodkin, J.: Fast pairwise structural RNA alignments by pruning of the dynamical programming matrix. *PLoS Comput Biol* **3**(10), 1896–1908 (2007). doi:[10.1371/journal.pcbi.0030193](https://doi.org/10.1371/journal.pcbi.0030193)
26. Sundfeld, D., Havgaard, J.H., de Melo, A.C., Gorodkin, J.: Foldalign 2.5: multithreaded implementation for pairwise structural RNA alignment. *Bioinformatics* **32**(8), 1238–1240 (2016). doi:[10.1093/bioinformatics/btv748](https://doi.org/10.1093/bioinformatics/btv748)
27. Middleton, S.A., Kim, J.: Nofold: RNA structure clustering without folding or alignment. *RNA* **20**(11), 1671–1683 (2014). doi:[10.1261/rna.041913.113](https://doi.org/10.1261/rna.041913.113)
28. Heyne, S., Costa, F., Rose, D., Backofen, R.: GraphClust: alignment-free structural clustering of local {RNA} secondary structures. *Bioinformatics* **28**(12), 224–32 (2012). doi:[10.1093/bioinformatics/bts224](https://doi.org/10.1093/bioinformatics/bts224)
29. Miladi, M., Junge, A., Costa, F., Seemann, S.E., Hull Havgaard, J., Gorodkin, J., Backofen, R.: RNAscClust: clustering RNA sequences using structure conservation and graph based motifs. *Bioinformatics* (2017). doi:[10.1093/bioinformatics/btx114](https://doi.org/10.1093/bioinformatics/btx114)
30. Wilm, A., Mainz, I., Steger, G.: An enhanced rna alignment benchmark for sequence alignment programs. *Algorithms for molecular biology* **1**(1), 1 (2006)
31. Havgaard, J.H., Torarinsson, E., Gorodkin, J.: Fast pairwise structural rna alignments by pruning of the dynamical programming matrix. *PLoS Comput Biol* **3**(10), 193 (2007)
32. Sundfeld, D., Havgaard, J.H., de Melo, A.C., Gorodkin, J.: Foldalign 2.5: multithreaded implementation for pairwise structural rna alignment. *Bioinformatics*, 748 (2015)
33. Washietl, S., Hofacker, I.L., Stadler, P.F.: Fast and reliable prediction of noncoding rnas. *Proceedings of the National Academy of Sciences of the United States of America* **102**(7), 2454–2459 (2005)
34. Gruber, A.R., Bernhart, S.H., Hofacker, I.L., Washietl, S.: Strategies for measuring evolutionary conservation of rna secondary structures. *BMC bioinformatics* **9**(1), 122 (2008)
35. Needleman, S.B., Wunsch, C.D.: A general method applicable to the search for similarities in the amino acid sequence of two proteins. *Journal of molecular biology* **48**(3), 443–453 (1970)
36. Suzuki, R., Shimodaira, H.: Pvclust: an r package for assessing the uncertainty in hierarchical clustering. *Bioinformatics* **22**(12), 1540–1542 (2006)
37. Ankerst, M., Breunig, M., Kriegel, H., et al.: Ordering points to identify the clustering structure. In: Proc. ACM SIGMOD, vol. 99 (1999)
38. Ester, M., Kriegel, H.-P., Sander, J., Xu, X., et al.: A density-based algorithm for discovering clusters in large spatial databases with noise. In: Kdd, vol. 96, pp. 226–231 (1996)
39. Van Nostrand, E.L., Pratt, G.A., Shishkin, A.A., Gelboin-Burkhart, C., Fang, M.Y., Sundararaman, B., Blue, S.M., Nguyen, T.B., Surka, C., Elkins, K., et al.: Robust transcriptome-wide discovery of rna-binding protein binding sites with enhanced clip (eclip). *Nature methods* **13**(6), 508–514 (2016)
40. Iyer, M.K., Niknafs, Y.S., Malik, R., Singhal, U., Sahu, A., Hosono, Y., Barrette, T.R., Prensner, J.R., Evans, J.R., Zhao, S., et al.: The landscape of long noncoding rnas in the human transcriptome. *Nature genetics* **47**(3), 199 (2015)
41. Hindorff, L.A., Sethupathy, P., Junkins, H.A., Ramos, E.M., Mehta, J.P., Collins, F.S., Manolio, T.A.: Potential etiologic and functional implications of genome-wide association loci for human diseases and traits. *Proceedings of the National Academy of Sciences* **106**(23), 9362–9367 (2009)
42. Ritchie, G.R., Dunham, I., Zeggini, E., Flück, P.: Functional annotation of noncoding sequence variants. *Nature methods* **11**(3), 294–296 (2014)

43. Gong, C., Maquat, L.E.: Lncrnas transactivate staufen1-mediated mrna decay by duplexing with 3'utrs via alu elements. *Nature* **470**(7333), 284 (2011)
44. Seemann, S.E., Mirza, A.H., Hansen, C., Bang-Bertelsen, C.H., Garde, C., Christensen-Dalsgaard, M., Torarinsson, E., Yao, Z., Workman, C.T., Pociot, F., et al.: The identification and functional annotation of rna structures conserved in vertebrates. *Genome Research*, 208652 (2017)
45. Will, S., Joshi, T., Hofacker, I.L., Stadler, P.F., Backofen, R.: Locarna-p: Accurate boundary prediction and improved detection of structural rnas. *Rna* **18**(5), 900–914 (2012)
46. Robin, X., Turck, N., Hainard, A., Tiberti, N., Lisacek, F., Sanchez, J.-C., Müller, M.: proc: an open-source package for r and s+ to analyze and compare roc curves. *BMC bioinformatics* **12**(1), 1 (2011)
47. Nawrocki, E.P., Eddy, S.R.: Infernal 1.1: 100-fold faster rna homology searches. *Bioinformatics* **29**(22), 2933–2935 (2013)
48. Muckstein, U., Hofacker, I.L., Stadler, P.F.: Stochastic pairwise alignments. *Bioinformatics* **18 Suppl 2**, 153–60 (2002)
49. Klein, R.J., Eddy, S.R.: RSEARCH: finding homologs of single structured RNA sequences. *BMC Bioinformatics* **4**, 44 (2003). doi:[10.1186/1471-2105-4-44](https://doi.org/10.1186/1471-2105-4-44)

Figures

Tables

Table 1: Comparative clustering performance.

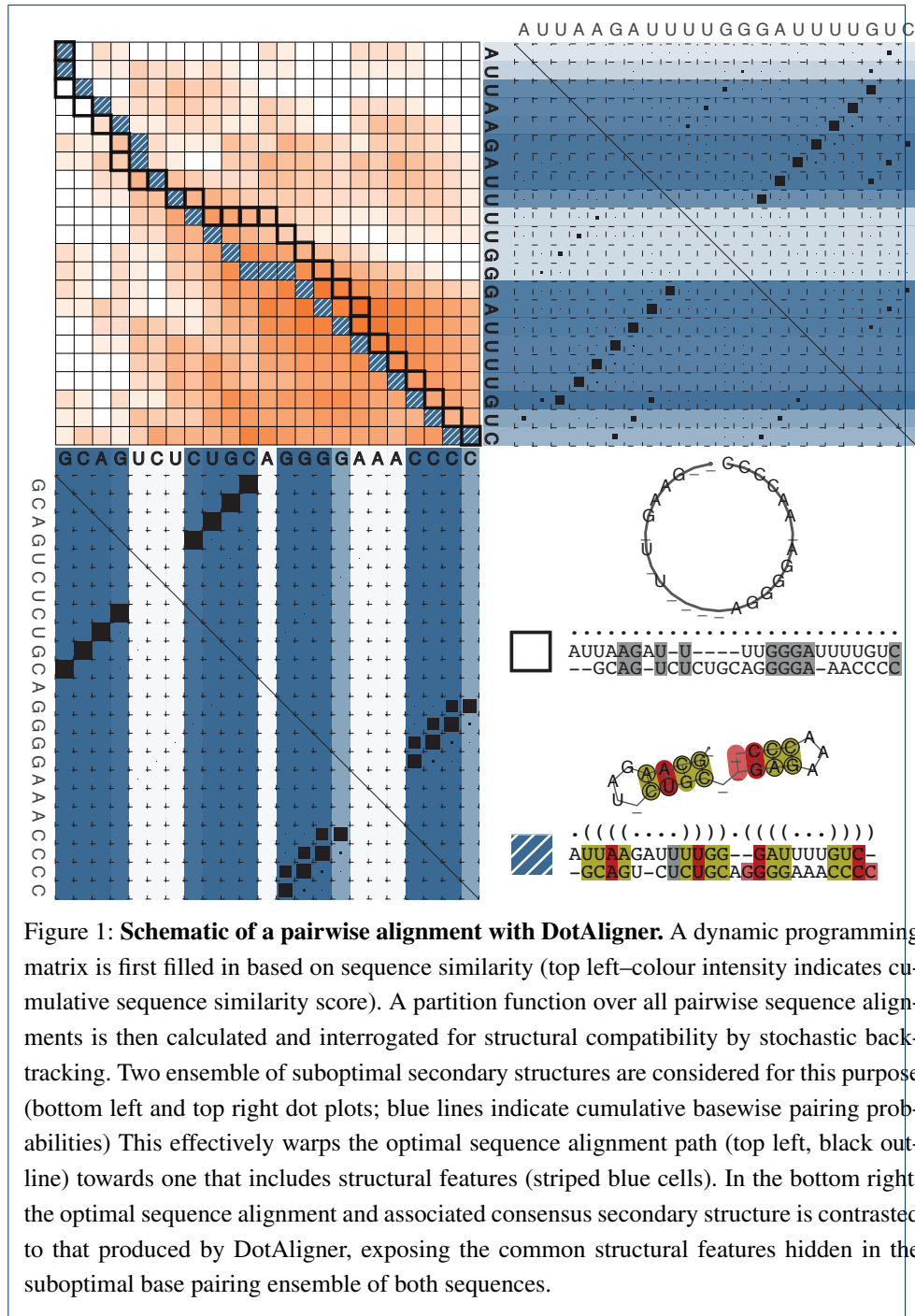
Algorithm	# Clusters	Sensitivity	Specificity	Accuracy
DotAligner+OPTICS	53	0.716	0.886	0.802
GraphClust	201	0.990	0.110	0.635
NoFold (all CMs)	62	0.866	0.965	0.916
NoFold (filtered)	45	0.674	0.976	0.826

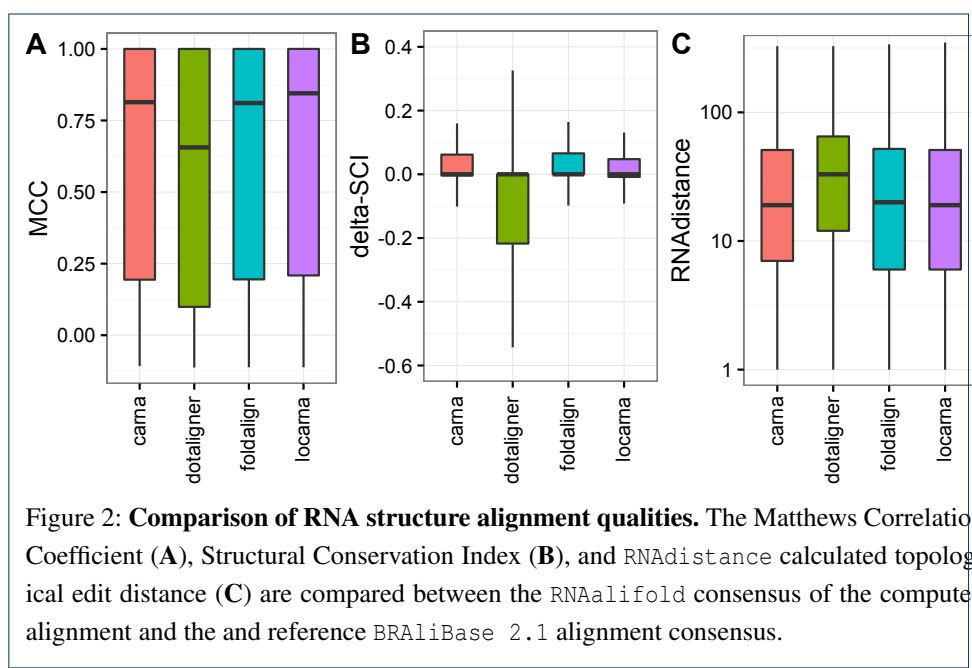
Additional files

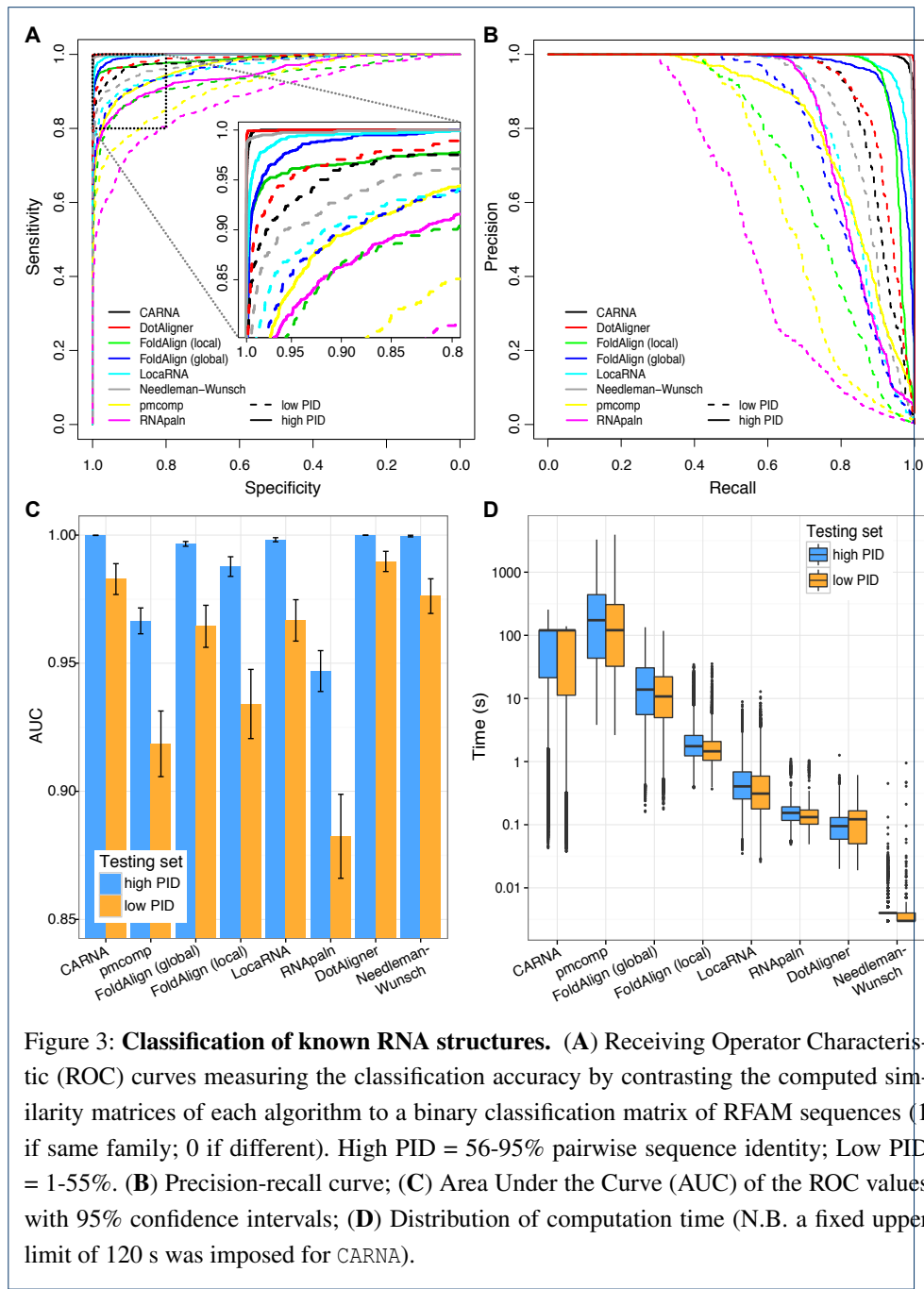
Additional file 1 — Supplementary methods

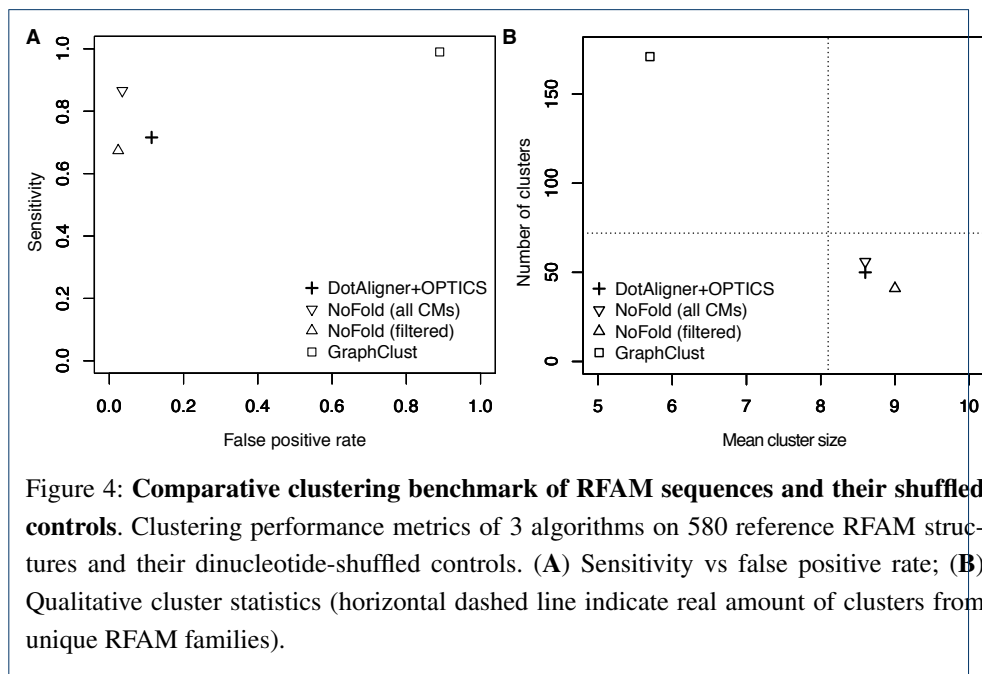
More detailed description of the DotAligner implementation, RNA structure clustering and eCLIP data processing.

Additional file 2 — Supplementary figures and tables









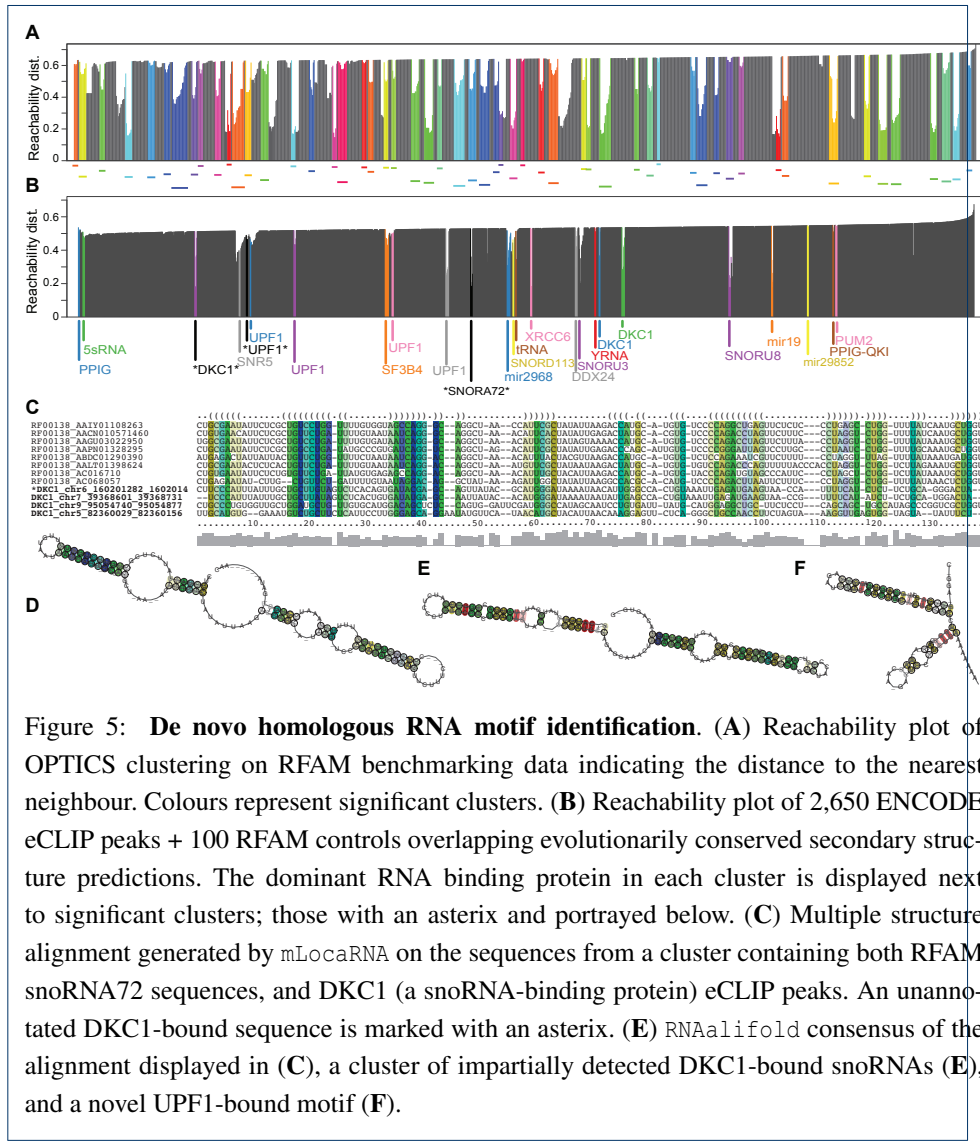


Figure 5: De novo homologous RNA motif identification. (A) Reachability plot of OPTICS clustering on RFAM benchmarking data indicating the distance to the nearest neighbour. Colours represent significant clusters. (B) Reachability plot of 2,650 ENCODE eCLIP peaks + 100 RFAM controls overlapping evolutionarily conserved secondary structure predictions. The dominant RNA binding protein in each cluster is displayed next to significant clusters; those with an asterisk and portrayed below. (C) Multiple structure alignment generated by mLocaRNA on the sequences from a cluster containing both RFAM snoRNA72 sequences, and DKC1 (a snoRNA-binding protein) eCLIP peaks. An unannotated DKC1-bound sequence is marked with an asterisk. (E) RNAalifold consensus of the alignment displayed in (C), a cluster of impartially detected DKC1-bound snoRNAs (E), and a novel UPF1-bound motif (F).

Additional file 1 — Supplementary methods

The pipelines, scripts and some programs used in this work can be found in the GitHub repository associated to this work at <https://github.com/noncodo/BigRedButton>.

1. DotAligner implementation

As described in [23] the weight W of alignment A of two arc-annotated sequences (S_a, P_a) and (S_b, P_b) is defined by

$$\begin{aligned} W(A) &= \sigma(A) + \tau(A) + \gamma(A) \\ &= \sum_{(i,i') \in A} \sigma(i, i') + \sum_{\substack{(i,j) \in P_a, \\ (i',j') \in P_b, \\ (i,i') \in A, \\ (j,j') \in A}} \tau(i, j, i', j') + \gamma \times N \end{aligned} \quad (1)$$

where S is a sequence and P is a base pairing probability matrix, $\sigma(i, i')$ is the similarity of sequence positions $S_a[i]$ and $S_b[i']$, $\tau(i, j, i', j')$ is the similarity of arcs $(i, j) \in P_a$ and $(i', j') \in P_b$, and γ is the gap cost associated with each sequence position that is not matched ($N = |S_a| + |S_b| - 2|A|$). The alignment problem finds the maximal $W(A)$. As its solution is MAX-SNP-hard, in praxis heuristics are used to find near-optimal solutions.

DotAligner solves the related problem of aligning two base pair probability matrices (dot plots). A major criteria for the implementation was a fast running time enable all-vs-all pairwise structural alignments and the associated distance (dissimilarity) matrix, which can be used for cluster analysis of large data sets [19]. Consequently, it employs a heuristic alignment-envelope, which imposes constraints to sub-optimal string alignments, and a fold-envelope, which imposes constraints to pre-calculated base pairing probabilities, to build pairwise sequence-structure alignments. DotAligner makes use of the observation that large samples from the ensemble of stochastic sequence alignments contain the correct structure-based alignment with significant probability, even though the optimal sequence alignment deviates significantly from the structural alignment [48].

Below, we describe the alignment procedure and weight functions. The alignment procedure consists of two steps:

- 1 Pairwise probabilistic string alignments;
- 2 Stochastic backtracking of string alignments and combining weights of base pairing probability matrices.

1.1 Pairwise probabilistic string alignments

In step 1 the computation of the partition function over all canonical pairwise string alignments is adapted from probA [48]. The probability of an alignment A in the ensemble of all alignments $Z(T)$ is

$$Pr(A; T) = \frac{1}{Z(T)} \exp(\beta W(A)), \quad (2)$$

where $\beta = 1/T$. The parameter T is analogous to the temperature in the thermodynamic interpretation of the alignment problem and determines the relative importance of the optimal

string alignment. If $T = 1$ then we recover the 'true' probability, if $T \rightarrow 0$ then $Pr(A; 0) = 0$ for all alignments with a score $W(A)$ less than the score of the optimal string alignment, and if $T \rightarrow \infty$ then all alignments have the same $Pr(A, \infty) = 1/Z(\infty)$. Hence, T controls the search space of suboptimal alignments for step 2. The algorithm runs in $O(N^3)$ for calculating the partition function. The weight function $W(A)$ of the probA implementation is changed to explore the ensemble of dot plot alignments. We reduce the sequence-structure alignment problem to a two-dimensional problem similar to the metric introduced in STRAL [22]. Hence, step 1 considers only the similarity σ and the gap cost γ described in equation 1:

$$W_{\text{Step1}}(A) = \sigma(A) + \gamma(A) \quad (3)$$

The similarity $\sigma(i, i')$ for matched sequence positions $S_a[i]$ and $S_b[i']$ takes into account sequence similarity M_{Seq} and the similarity in their unpaired probabilities $\Delta\omega(i, i')$ weighted by the parameter θ :

$$\sigma(i, i') = \theta \times M_{\text{Seq}}^{(i, i')} + (1 - \theta) \times \Delta\omega(i, i') \quad (4)$$

$M_{\text{Seq}}^{(i, i')}$ is 1 if sequence positions $S_a[i]$ and $S_b[i']$ match and else 0. The similarity of unpaired probabilities is defined as

$$\Delta\omega(i, i') = \begin{cases} 0 & \text{if } \omega(i) == 0 \\ & \text{and } \omega(i') == 0 \\ 1 - |\omega(i) - \omega(i')| & \text{else} \end{cases} \quad (5)$$

so that $\Delta\omega = (0, 1)$. Alternatively a statistical substitution model R_{Seq} replaces the sequence similarity and is multiplied with the ζ weighted sum of $\Delta\omega$ and the similarity in ratios of upstream pairing probability $\Delta\omega^{up}$:

$$\sigma(i, i') = R_{\text{Seq}}^{(i, i')} \times \zeta \times \Delta\omega(i, i') + R_{\text{Seq}}^{(i, i')} \times (1 - \zeta) \times \Delta\omega^{up}(i, i') \quad (6)$$

R_{Seq} is a 4×4 matrix of probabilities for observing a given substitution relative to background nucleotide frequencies. We use the log-odd scores L from the RIBOSUM85-60 matrix introduced in [49] which are transformed to probabilities R_{Seq} by $2^{L(i, i')}/(1 + 2^{L(i, i')})$. The ratio of upstream pairing probability ω^{up} is defined as

$$\omega^{up}(i) = \sum_{k=1}^{i-1} \psi(k, i) / \sum_{k=1}^{|S|} \psi(k, i) \quad (7)$$

where $i \in S$, $|S|$ is the length of sequence S , and $\psi(k, i)$ is the pairing probability of sequence positions $S[k]$ and $S[i]$. The downstream pairing probability is implicitly considered in the

weight function through the usage of unpaired probability and upstream pairing probability. The gap term in equation 1 is replaced with affine gap costs:

$$\gamma(A) = l \times g_o + (N - l) \times g_{ext} \quad (8)$$

where l is the number of initiation gaps, N is the number of all gaps, g_o is the penalty for opening a gap and g_{ext} is the penalty for gap extensions. Start and end gaps are considered as free.

1.2 Stochastic backtracking and combined weight of dot plot alignments

Here, a properly weighted sample of stochastic pairwise string alignments in the alignment ensemble is examined across both sequences for sequence-structure similarity. The stochastic backtracking is adapted from probA [48] for selecting s suboptimal string alignments A_s . The combined weight W_{Step2} is a variant of equation 1 to explore the similarity of the corresponding dot plot alignments:

$$W_{\text{Step2}}(A_s) = \kappa \times \frac{W_{\text{Step1}}(A_s)}{|A_s|} + (1 - \kappa) \times \frac{\tau(A_s)}{|\text{Match}_{A_s}|^2} \quad (9)$$

where the parameter κ weights for each alignment A_s between the sequence-based similarity $W_{\text{Step1}}(A_s)$ normalised by alignment length $|A_s|$ and dot plot similarity $\tau(A_s)$ normalised by the number of aligned bases $|\text{Match}_{A_s}|$ in alignment A_s . Similar to equation 4 the dot plot similarity τ sums the parameter θ weighted similarity of aligned base pairs M_{paired} and the similarity in their pairing probabilities $\Delta\psi$:

$$\tau(i, j, i', j') = \theta \times M_{\text{paired}}^{(i, j, i', j')} + (1 - \theta) \times \Delta\psi(i, j, i', j') \quad (10)$$

where $M_{\text{paired}}^{(i, j, i', j')}$ is 1 if $S_a[i]$ and $S_a[j]$ as well as $S_b[i']$ and $S_b[j']$ form canonical base pairs (G-C, C-G, A-U, U-A, G-U or U-G) and else 0. The similarity in pairing probabilities $\Delta\psi$ is then calculate by

$$\Delta\psi(i, j, i', j') = \begin{cases} 0 & \text{if } \psi(i, j) == 0 \text{ and } \psi(i', j') == 0 \\ 1 - |\psi(i, j) - \psi(i', j')| & \text{else} \end{cases} \quad (11)$$

Similar to M_{Seq} in equation 4, the base pair similarity matrix M_{paired} can be replaced by a statistical substitution model R_{paired} which describes the probability for observing a given base pair substitution relative to background nucleotide frequencies:

$$\tau(i, j, i', j') = R_{\text{paired}}^{(i, j, i', j')} \times \Delta\psi(i, j, i', j') \quad (12)$$

Again, the log-odd scores L from the RIBOSUM85-60 matrix [49] are transformed to probabilities R_{paired} .

For both sequences S_a and S_b , the pairing probability matrices P_a and P_b are computed in advance using McCaskill's algorithm, implemented in RNAfold or RNAlignfold. The robustness of the alignment is improved by applying log-odds scores ψ of having a specific base pairing against the null model of a random pairing [19]:

$$\psi(i, j) = \max \left(0, \log \frac{P(i, j)}{p_0} / \log \frac{1}{p_0} \right) \quad (13)$$

where p_0 is the expected probability for a pairing to occur at random. The term $\log \frac{1}{p_0}$ is a normalization factor that transforms the scores to a maximum of 1. $P == 1$ results in $\psi = 1$, $P > p_0$ results in $\psi > 0$, and $P \leq p_0$ results in $\psi = 0$. This transformation gives weaker similarities if low base pair probabilities are compared, but stronger similarities for high base pair probabilities. Unpaired probabilities are handled in a similar way by

$$\omega(i) = \max \left(0, \log \frac{1 - \sum_k P(i, k)}{p_0} / \log \frac{1}{p_0} \right) \quad (14)$$

where p_0 is the expected probability for an unpaired base to occur at random.

2. Clustering RNA structures with randomised controls

Below is the code used to calculate the accuracy and other performance metrics of the clustering benchmark of stochastically sampled RFAM entries. All files can be found on the associated GitHub repository <https://github.com/noncodo/BigRedButton>.

```
cat("File name", "TP", "TN", "FP", "FN", "SENS", "SPEC", "ACC", "\n", sep="\t",
    file="accuracies.tsv")
file.names <- dir(pattern="*_clust.tsv$")
for(x in 1:length(file.names)){
  gc <- read.delim(file.names[x], header=F)
  # for 1 - max V2
  TP=0
  FP=0
  NumClust <- max(gc$V2)
  for ( cl in 0:NumClust) {
    if ( cl %in% gc$V2 ) {
      v <- as.vector( gc$V1[ gc$V2 == cl ] )
      t <- sort( table( v ), decreasing=T )
      best <- as.integer( t[1] )
      cID <- names( t[ 1 ] )
      if ( cl == 0 ) {
        if ( cID == "shuffled" ) {
          FN <- length(v)-best
          TN <- best
        }
        else
          cat("Houston, we have a TN problem")
      }
      else {
        if ( cID == "shuffled" ) {
```

```

        FP = FP + length(v)
    }
    if ( is.na( as.integer( t[2] ) ) || as.integer( t[2] ) < best ) {
        TP = TP + best
        FP = FP + length(v)-best
    }
    else if ( as.integer( t[2] ) == best ) {
        # treat both as false positives
        FP = FP + length(v)
    }
}
}
TP
TN
FP
FN
SENS=TP / (TP + FN )
SENS
SPEC=TN / ( TN + FP )
SPEC
ACC=(TP + TN) / ( TP + TN + FP + FN )
ACC
cat(file.names[x],TP,TN,FP,FN,SENS,SPEC,ACC, "\n",sep="\t",
     file="accuracies.tsv", append=T)
}

```

3. eCLIP data processing

Data in .bigBed format was acquired from the ENCODE data hub from the following link:
https://www.encodeproject.org/search/?type=Experiment&assay_term_name=eCLIP&files.file_type=bigBed+narrowPeak&month_released=April%2C+2016

```

# Convert accessions to protein IDs
cut -f 1,16,29 metadata.tsv | sed 's/-human _/g' | while read line
do
    F1=$(echo $line | awk '{print $1".bed"}')
    F2=$( echo $line | awk '{ print $2".bed"}')
    cp $F1 $F2
done

# Rename files accordingly
for file in *bed
do
    mv $file $(head -n 1 $file | cut -f 4).bed
done

# Filter for greater than or equal to 8x fold enrichment
# And -log10( P-value ) greater than or equal to 4
for file in *rep0?.bed
do
    awk '{if ($7 >= 4 && $8 >= 4) print }' $file > ../filtering/${file}_filt3
done

#Intersect both replicates (>1 overlap)
for file in *rep01.bed_filt3 ; do
    >&2 echo "Processing "$file
    bedtools intersect -s -u -f 0.5 -a <( cut -f 1-6 $file ) -b <( cut -f 1-6
    ${file//rep01/rep02} ) > ${file}_1

```

```
bedtools intersect -s -u -f 0.5 -b <( cut -f 1-6 $file ) -a <( cut -f 1-6
${file//rep01/rep02} ) > ${file}_2

# merge peaks if they are close together
bedtools merge -d 50 -s -delim " | " -c 4,5,6 -o first,count,first -i <( cat
${file}_1 ${file}_2 | sort -k 1,1 -k 2,2n ) >
${file%*.bed_filt3}_filt_0.5_merged_50_s.bed

# intersect with ECS (in file ECS_congruous_sorted.bed6)
bedtools intersect -wo -s -b ${file%*.bed_filt3}_filt_0.5_merged_50_s.bed
-a ECS_congruous_sorted.bed6 >
${file%*.bed_filt3}_filt_0.5_merged_50_s_anyECS.bed
done

#merge all files into one
cat *_50_s_anyECS_merged.bed > All_ECS_merged_50nt_peaks.bed
# wc -l All_ECS_merged_50nt_peaks.bed
## 2650

#edit sequence names and get sequence from reference genome (hg19)
awk 'OFS="\t">{print $1,$2,$3,$4"_"$1"_"$2"_"$3"_"$6,$5,$6}'
./All_ECS_merged_50nt_peaks.bed > ./All_ECS_merged_50nt_peaks_renamed.bed
bedtools getfasta -s -name -fi ~/data/fasta/hg19.fa -bed
./All_ECS_merged_50nt_peaks_renamed.bed -fo
./All_ECS_merged_50nt_peaks_renamed.fasta

#combine with known control RNA structure
cat All_ECS_merged_50nt_peaks_renamed.fasta spike-ins.fasta >
All_ECS_merged_50nt_peaks_renamed_spikeIns.fasta
```

Additional file 2 — Supplementary Tables and Figures

Supplementary Table 1. List of RFAM families from benchmark that did not cluster

Sequence count	RFAM ID	RFAM family
2	RF00005	tRNA
5	RF00015	U4 spliceosomal RNA
8	RF00020	U5 spliceosomal RNA
5	RF00021	Spot 42 RNA
1	RF00026	U6 spliceosomal RNA
10	RF00059	TPP riboswitch (THI element)
5	RF00167	Purine riboswitch
11	RF00169	Bacterial small signal recognition particle RNA
13	RF00199	SL2 RNA
4	RF00374	Gammaretrovirus core encapsidation signal
11	RF00378	Qrr RNA
6	RF00386	Enterovirus 5' cloverleaf cis-acting replication element
6	RF00389	Bamboo mosaic virus satellite RNA cis-regulatory element
4	RF00444	PrrF RNA
17	RF00494	Small nucleolar RNA U2-19
2	RF00515	PyrR binding site
4	RF00550	Hepatitis E virus cis-reactive element
7	RF01685	6S-Flavo RNA
7	RF01697	Chlorobi-RRM RNA
6	RF01705	Flavo-1 RNA
4	RF01725	SAM-I/IV variant riboswitch
2	RF01728	STAXI RNA
7	RF01734	crcB RNA
1	RF01750	pfl RNA
6	RF01754	radC RNA
4	RF01764	yjdF RNA
5	RF02033	HNH endonuclease-associated RNA and ORF (HEARO) RNA

Supplementary Table 2. List of control RNA structures

Sequences	RNA family	RFAM ID
5	5SRNA	RF00002
8	SNORA72	RF00138
10	SNORD113	RF00181
10	SNORU3	RF00012
10	SNORU8	RF00096
8	SNR5	RF01252
9	YRNA	RF00019
10	mir19	RF00245
7	mir2968	RF02093
6	mir29852	RF02095
17	tRNA	RF00005

Supplementary Table 3. Rank-product of best DotAligner parameters

Parameters	low_PI rank	high_PI rank	rank product	low_PI AUC	high_PI AUC	AUC sum	Combined Time
T=10 s=1 k=0.3 t=0.5 o=1 e=0.05	1	112	112	0.983297903	0.996178994	1.97948	0.140273
T=1 s=1 k=0.3 t=0.8 o=1 e=0.05	181	1	181	0.959342489	0.997188985	1.95653	0.133496
T=1 s=1 k=0.3 t=0.5 o=1 e=0.05	2	110	220	0.983297903	0.996178994	1.97948	0.135262
T=5 s=1 k=0.3 t=0.5 o=1 e=0.05	3	109	327	0.983297903	0.996178994	1.97948	0.134188
T=10 s=5 k=0.3 t=0.8 o=1 e=0.05	184	2	368	0.959342489	0.997188985	1.95653	0.144565
T=1 s=5 k=0.3 t=0.5 o=1 e=0.05	4	113	452	0.983297903	0.996178994	1.97948	0.150288
T=10 s=1 k=0.3 t=0.8 o=1 e=0.05	182	3	546	0.959342489	0.997188985	1.95653	0.142137
T=10 s=5 k=0.3 t=0.5 o=1 e=0.05	5	114	570	0.983297903	0.996178994	1.97948	0.156738
T=5 s=5 k=0.3 t=0.5 o=1 e=0.05	6	111	666	0.983297903	0.996178994	1.97948	0.155101
T=5 s=1 k=0.3 t=0.8 o=1 e=0.05	185	4	740	0.959342489	0.997188985	1.95653	0.146729
T=10 s=20 k=0.3 t=0.5 o=1 e=0.05	7	115	805	0.983297903	0.996178994	1.97948	0.186257
T=5 s=20 k=0.3 t=0.5 o=1 e=0.05	8	116	928	0.983297903	0.996178994	1.97948	0.192388
T=1 s=5 k=0.3 t=0.8 o=1 e=0.05	186	5	930	0.959342489	0.997188985	1.95653	0.154183
T=1 s=20 k=0.3 t=0.5 o=1 e=0.05	9	117	1053	0.983297903	0.996178994	1.97948	0.210514
T=5 s=5 k=0.3 t=0.8 o=1 e=0.05	183	6	1098	0.959342489	0.997188985	1.95653	0.154234
T=10 s=50 k=0.3 t=0.5 o=1 e=0.05	10	119	1190	0.983297903	0.996178994	1.97948	0.285647
T=5 s=1 k=0.4 t=0.6 o=1 e=0.05	13	97	1261	0.983273039	0.996343919	1.97962	0.133738
T=5 s=50 k=0.3 t=0.5 o=1 e=0.05	11	118	1298	0.983297903	0.996178994	1.97948	0.269801
T=10 s=20 k=0.3 t=0.8 o=1 e=0.05	187	7	1309	0.959342489	0.997188985	1.95653	0.187293
T=10 s=1 k=0.4 t=0.6 o=1 e=0.05	14	101	1414	0.983273039	0.996343919	1.97962	0.144514

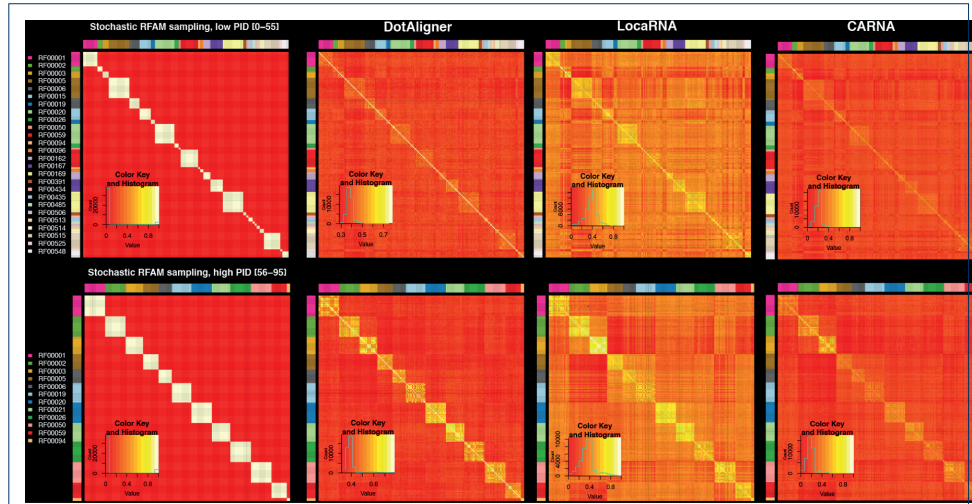


Figure S1. Binary classification of similarity matrices

Stochastically sampled RFAM sequences are labelled as belonging to the same family in white, and in red when not (Left). Heatmaps of the similarity matrices produced by DotAligner, LocaRNA and CARNA are listed in columns 2, 3 and 4, respectively. (top) Low mean pairwise identity samples, where each sequence within a family shares between 0 and 55% sequence identity; (bottom) Higher (56–95%) mean pairwise identity samples.

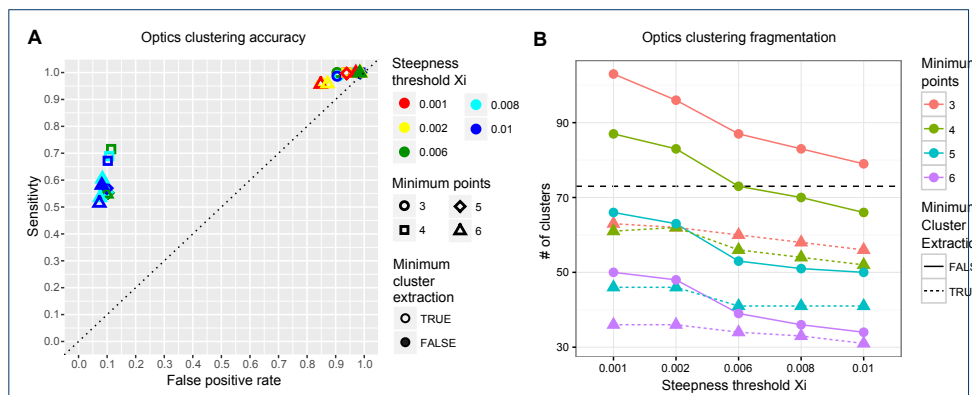


Figure S2. OPTICS clustering optimisation

Effect of OPTICS parameters on clustering accuracy (A) and amount of clusters (B) from a DotAligner dissimilarity matrix of 580 reference RFAM structures and their dinucleotide-shuffled controls (horizontal dashed line indicates expected amount of clusters, or unique RFAM families).

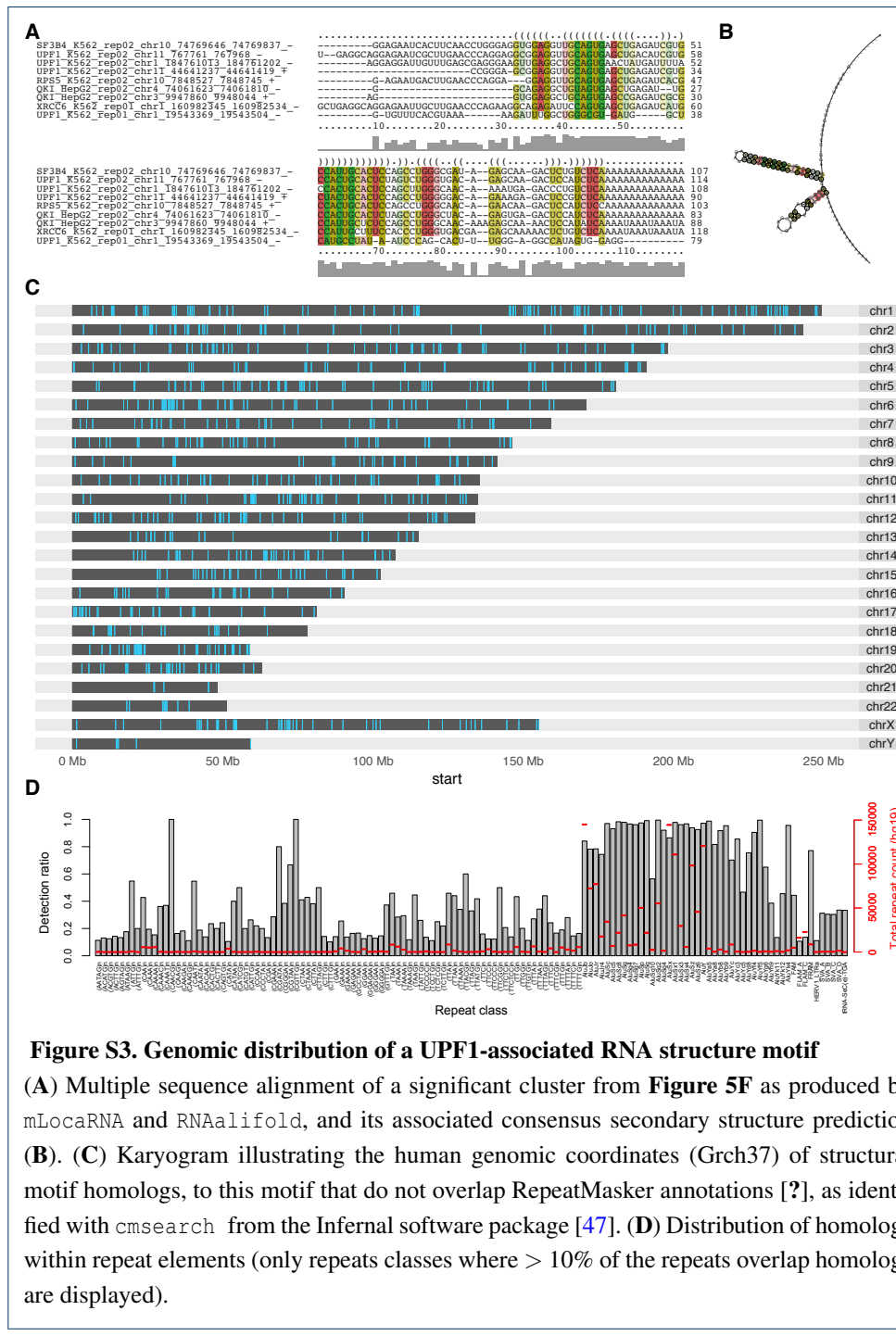


Figure S3. Genomic distribution of a UPF1-associated RNA structure motif

(A) Multiple sequence alignment of a significant cluster from **Figure 5F** as produced by mLocaRNA and RNAalifold, and its associated consensus secondary structure prediction (B). (C) Karyogram illustrating the human genomic coordinates (Grch37) of structural motif homologs, to this motif that do not overlap RepeatMasker annotations [?], as identified with cmsearch from the Infernal software package [47]. (D) Distribution of homologs within repeat elements (only repeats classes where > 10% of the repeats overlap homologs are displayed).